A sodiophilic amyloid fibril modified separator for dendrite-free sodium metal batteries.

WANG, J., GAO, Y., LIU, D., ZOU, G., LI, L., FERNANDEZ, C., ZHANG, Q. and PENG, Q.

2024

Sodiophilic amyloid fibril modified separator for dendrite-free sodium metal batteries

*Jinming Wang, Yan Gao, Di Liu, Guodong Zou, Lanjie Li, Carlos Fernandez, Qingrui Zhang, Raffaele Mezzenga, Qiuming Peng**

J.M. Wang, Y. Gao, D. Liu, G.D. Zou, Q.R. Zhang, Q.M. Peng

State Key Laboratory of Metastable Materials Science and Technology, Yanshan University, Qinhuangdao, 066004, P.R. China

Corresponding Authors: pengqiuming@ysu.edu.cn

L.J. Li

Chengde Iron and Steel Group Co., Ltd, HBIS Group Co., LTD., Chengde, Hebei 067102, China

C. Fernandez

School of Pharmacy and Life Sciences, Robert Gordon University, Aberdeen, AB107GJ, United Kingdom

R. Mezzenga

Laboratory of Food and Soft Materials, Department of Health Sciences and Technology, ETH Zurich, Schmelzbergstrasse 9, Zurich 8092, Switzerland

Keywords: amyloid fibril; Na metal battery; amino acids; electric field distribution; SEI composition

Abstract

Sodium (Na) batteries are being considered as prospective candidates for the next generation of secondary batteries in contrast to lithium-based batteries, due to their high raw material abundance, low cost, and sustainability. However, the unfavorable growth of Na metal deposition and severe interfacial reactions have prevented their large-scale applications. Here we propose a vacuum filtration strategy through amyloid fibril modified glass fiber separators to address these issues. The modified symmetric cell can be cycled for 1800 h, surpassing the performance of previously reported Na-based electrodes under an ester-based electrolyte. Moreover, the Na/ $Na_3V_2(PO_4)_3$ full cell with a sodiophilic amyloid fibril modified separator exhibits a capacity retention of 87.13% even after 1000 cycles. Both experimental and theoretical results show sodiophilic amyloid fibril homogenizes electric field and Na ion concentration, fundamentally inhibiting dendrite formation. Simultaneously, the glutamine amino acids in the amyloid fibril have the highest adsorption energy for Na, resulting in the formation of a stable Na_3N and NaN_xO_y-rich solid electrolyte interface film on the anode during cycling. This work provides not only a possible

pathway to solve dendrite problem in metal batteries using environmental-friendly biomacromolecular materials, but also a new direction for expanding biomaterial applications.

1. Introduction

The dramatic growth of high-power electronic devices, coupled with the fact that traditional Li ion batteries are nearly approaching their theoretical energy density limitation, has prompted enthusiasm for more advanced batteries.[1-2] Undoubtedly, the direct application of alkali metals as anodes is a promising strategy for increasing the theoretical specific capacity.[3] Theortically, the natural abundance of Na in the earth crust (23.6×10^3 ppm) is three orders of magnitude greater than that of Li (20 ppm).[4] However, the uncontrolled growth of Na dendrites in the presence of commercial ester-based electrolytes results in low Coulombic efficiency (CE), inferior cycling performance and even safety concerns after long-term cell operation.[5]

To accelerate the commercialization of rechargeable Na metal batteries, it is crucial to address the serious issues caused by dendrite growth. Basically, dendrite inhibition can be achieved through modifications of three battery components: the anode, the electrolyte and the separator. Among them, anodic modification can be used to build 3D host structures or to apply sodiophilic coatings to inhibit dendrites.[6-7] Nevertheless, anodic modification frequently raises significant safety concerns due to the high activity of Na.[8] In contrast, electrolyte modification can be achieved by adding additives,[9] althoughs solid electrolyte interface (SEI) film formed using electrolyte additives are relatively stable but does not completely prevent dendrite penetration, especially after long-term cycling.[10] Noticeably, the separator is an essential component of the battery and directly affects safety performance. Therefore, the modification of separators to prevent dendrite penetration is an

important and promising strategy.[11] However, it is well known that uneven electric field distributions and ion concentration distributions inevitably form within the pores in the separator during the deposition of Na.[12] Additionally, both Na ions and electric fields tend to focus at protrusions with high surface energy.[13] As a result, Na nucleation and growth tend to occur more commonly at tip sites, leading to non-uniform Na deposition. The formation of Na protrusions further enhances the strength of the local electric field surrounding them, causing Na protrusions to evolve into Na dendrites during cycling.[14] This phenomenon is more serious in ester-based electrolytes due to the difficulty forming stable SEI films on the anode surface.[15] Consequently, physical modification based on the separator perspective is better than anode modification to improve the electric field distribution and stabilize Na batteries.

Biomacromolecular structures such as proteins are enriched with polar groups can homogenize ionic fluxes and induce uniform metal deposition.[16] For example, modified soybean protein fibers provide a good modulation of Li deposition by forming a LiF-rich SEI membrane.[17] Besides, collagen hydrolysate induces a deionization shock and diffuses cations on Li or Zn anode to promote homogeneous metal deposition.[18] However, there is still a lack of interpretation on how protein molecules affect metal deposition and SEI components, and in particular which amino acids play an crucial impact during repeated cycles.

Herein, we propose that filtering a uniform layer of amyloid fibrils (AF) over the separator physically induces a uniform electric field and Na^+ concentration, which fundamentally inhibits the formation of dendrites, and additionally generates a stable SEI film further stabilizing the Na metal anode. Specifically, we found that the addition of AF allowed an increased proportion of Na-dense crystalline surfaces to occur during Na deposition, which enhanced the reversibility of the Na metal

battery. We also discover that glutamine amino acids in amyloid fibrils have the highest binding energy for Na , resulting in the presence of a Na_3N and NaN_xO_y rich SEI film during cycling, and then it improves the interface generated by the ester-based electrolyte on the anode surface. Therefore, a unique dendrite-free metal deposition has been achieved in terms of physical fiber structure and chemical composition modulation in the amyloid fibrils. In this case, the symmetrical Na metal batteries remain stable cycle over 1800 h, which is nearly 6 times higher than that of unmodified battery. Moreover, the capacity retention rate of amyloid fibrils modified Na metal full cells coupled with the high load cathode ($Na_3V_2(PO_4)_3$) can provide 87.13% high capacity retention rate even after 1000 cycles, which are far higher than those of the unmodified counterparts (69.46% after 200 cycles).

2. Results and Discussion

2.1. Preparation of Amyloid Fibrils@Glass Fiber Separator

The amyloid fibrils@glass fiber (AF@GF) separator was prepared in two steps: the synthesis of amyloid fibrils in combination with the vacuum filtration of amyloid fibrils onto the GF separator (**Figure 1a, Figure S1, Supporting Information**). Typically, we firstly prepared amyloid fibrils containing a variety of amino acids through a series of methods such as acid washing, dialysis and hydrolysis based on the abundance of amyloid fibrils in β-lactoglobulin, as described in the materials preparation section. Fourier-transform infrared (FT-IR) spectroscopy is used to analyze the AF1, AF5, and AF10 samples, which are produced by hydrolysis for 1, 5, and 10 hours, respectively (**Figure 1b**). The typical protein absorption peaks at 1649.1 cm^{-1} and 1535.3 cm^{-1} are observed, assigning to amide I (C=O stretching) and amide III (N-H in-plane bending/C-N stretching), respectively. These

peaks are mainly associated with the vibrations of peptide bonds in the AF samples. [19-20] Additionally, other absorption peaks at 1450.4 cm^{-1} ($C-H_{2/3}$), 1234.4 cm^{-1} (C-O stretching), 2964.5 cm^{-1} ($C-H_3$), 3292.3 cm^{-1} (O-H) and 3411.9 cm^{-1} (N-H) are also demonstrated.[21-22] The abundance of polar groups in the AF5 is expected to effectively reduce the concentration polarization in Na metal battery.[23] The presence of N in the AF5 is demonstrated by the amide/NH_3^+ at 400.1eV and N-H/C-N at 399.7eV in the N*1s* spectrum, while the presence of C and O is chiefly in the form of C-C, C=O, C-O, and O-H (**Figure 1c, Figure S2, Supporting Information**).[19, 24] Furthermore, Raman spectroscopy indicates that the amide I band at 1669.3 cm^{-1} in the AF5 is considered to be the C=O bond, relative to the absorption of amide I being caused by the stretching vibration of the short C=O bond in protein (**Figure 1d**).[25] The other characteristic peaks at 1449.7 and 1238.6 cm^{-1} are assigned to the presence of amide III, in terms of C-N stretching and N-H bending vibrations of the peptide bond.[26]

Morphology variation of the produced amyloid fibrils was further investigated by transmission electron microscope (TEM), in which the hydrolysis time remarkably affects morphologies of the amyloid fibrils (**Figure 1e, Figure S3, Supporting Information**). Specifically, the dimensions of the AF5 (hydrolysis time for 5 h)are approximately 3.3 μm in length and 12.4 nm in diameter, but the length and diameter values of the AF1 change to 1.3 μm and 42 nm, respectively. Worse, the morphology of the AF10 is indistinguishable, probably due to long hydrolysis time leading to amyloid fibrils agglomeration and breakage.[27] In this regard, the AF5 may expose more surface groups compared with other samples. After the AF5 has been prepared, it is decorated to the GF separator by vacuum filtration. During the compounding process, the ionic conductivity (σ) of AF5@GF decreases slightly in contrast to that of the GF separator, but the GF does not react with the AF5 to form new substances **(Figure S4, Supporting Information)**. Scanning electron microscope (SEM) images reveal

that the amyloid fibrils deposited on the GF separator exhibits a disordered morphology. Notably, the amyloid fibrils agglomerate on the surface due to fibril gelation **(Figure S5, Supporting Information)** when the concentration of the amyloid fibril solution is 5 wt.%. The SEM and energy-dispersive X-ray spectroscopy (EDS) data reveal that the thickness of the deposited amyloid fibril is 1, 5 and 10 μm, with the AF5 concentrations of 1, 2 and 5 wt.%, respectively **(Figure 1f-j, Figure S6, Supporting Information)**. According to these observations, we selected an amyloid fibril concentration of 2 wt.% for subsequent testing, which can achieve more uniform and abundant amyloid fibril deposition but avoiding fibril gelation.

To further assess the effects of amyloid fibril on separator intrinsic properties, we investigated their related physical properties, such as wettability, mechanical properties, elastic modulus and adhesion force. Both separators are found to be wettable by the liquid electrolyte (1.0 M $NaClO_4$ in EC:DEC=1:1 vol.% with 5.0 wt.% FEC), with initial contact angles of 28.4º and 34.8º for the GF separator and the AF5@GF composite separator, respectively. (**Figure S7,Video S1, 2, Supporting Information**). Additionally, the stress-strain curves (**Figure S8, Supporting Information**) display the tensile strength of the AF5@GF separator is approximately 5.1 times higher than that of the commercial GF separator. Meanwhile, the elastic modulus is improved remarkably. This trend has further confirmed by atomic force microscopy (AFM) *via* quantitative nano-mechanics mode, wherein the elastic modulus of the AF5@GF separator surface is found to be about 25.2 ± 0.6 MPa, which is higher than that of the GF separator, at 13.9 ± 0.8 MPa. Besides, the adhesion force of the AF5@GF separator has enhanced at least 3.5 times higher than that of the GF separator (**Figure S9, Supporting Information**). These findings demonstrate that the AF5@GF separator exhibits superior

mechanical resistance and excellent puncture resistance, which might effectively prevent Na dendrites from penetrating the separator.[28]

2.2. Sodium Deposition

To probe Na deposition behavior of separator, we studied the reversibility of Na plating/stripping for the Na|Al asymmetric batteries with the GF separator or the AF5@GF separator in a conventional ester-based electrolyte. TEM and FTIR test results show that there is no significant change in the morphology and functional groups of AF5 after immersion in the electrolyte for 24 hours, implying that the AF5 is stable in the electrolyte (**Figure S10, Supporting Information**). As shown in **Figure 2a and Figure S11**, the CEs of the Na|Al batteries with the GF separator exhibit a slow rise for approximately 30 cycles followed by a decline, and the average CEs remain at a low value of 68.8% during the initial 50 cycles, when operated at 0.5 mA cm^{-2} and 1 mAh cm^{-2}. However, the Na|Al batteries with the AF5@GF separator can run for 150 cycles with an average CE of 91.6%. In addition, the nucleation overpotential of the Na|Al battery assembled with the AF5@GF separator is only 0.245 V, which is 9% lower than the bare GF separator, signifying that the deposition barrier of Na ion on the former can be reduced on the electrode (**Figure 2b**).

The performance of the AF5@GF separator is better than that of the GF separator, which may be associated with the deposition morphology of Na.[12, 18] The difference in Na deposition morphology with and without the AF5 modification has been clarified by *in-situ* XRD, SEM and COMSOL simulations. On the one hand, *in-situ* XRD patterns show that the proportion of (110) crystal plane deposition of Na after the AF5 modification increased to 77.39%, while the proportion of low index (200) crystal plane decreased to 22.61% (**Figure 2c-e**). The increased proportion of

close-packed face of the deposited metal enhances the density of deposition and thus improves the reversibility of the batteries, which is consistent with the phenomenon existing in other metal batteries. [29-30] On the other hand, SEM images of Al current collector retrieved from the cycled Na|Al batteries display inhomogeneous loose structure with Na dendrites on Al current collectors using the bare GF separators at a deposition capacity of 1 mA cm^{-2} (**Figure 2f**). Such incompact structures may be related to the inhomogeneous nucleation and deposition of Na caused by the uneven distribution of the electric field.[12] Subsequently, Na dendrites are further evolved by the non-uniform deposition of Na through a self-amplifying mechanism (**Schematic 1**). On the contrary, dendrite-free deposition morphology on the Al collector in the Na|Al battery assembled with the AF5@GF separator is observed (**Figure 2g, Schematic 1**). Moreover, the corresponding SEM image of the AF5@GF verifies that Na deposition might be achieved on this separator, while the pristine GF separator is still dendritic Na appears (**Figure 2h-i**). Finally, two-dimensional finite element models are constructed to characterize the ion migration, electric field distribution and dendrite growth near the electrodes. The dendrites with a diameter of 0.5 μm are taken to compare the dendrite growth on the electrode with and without amyloid fibrils at the initial state. The governing equations are as follows:[31-32]

$$N_i = -D$$

where N_i is the mass flux for each species, D_i is the diffusion coefficient, c_i is the concentration, z_i is the charge number, V is the electrolyte potential, F is Faraday constant. Convection is not considered in this process, so u is 0. The model is solved in the solver COMSOL multiphasic. Overall, COMSOL simulations show that severe Na^+ polarization and electric field inhomogeneity occur in the AF5-free modified Na batteries after 500 min, leading to free growth of Na dendrites (**Figure 2j-k, Figure**

S12a-d, Supporting Information). In turn, the local Na^+ concentration of the battery model modified by the AF5 is obviously uniform, and the local electric field strength is ameliorated, which effectively inhibits the dendrite formation caused by mass transport and enhances sodium ion flux. (**Figure 2l-m, Figure S12e-h, Supporting Information**), in line with the XRD and SEM results. Besides, the calculated Na^+ transference number (t_{Na+}) for the AF5@GF is 0.82, which is slightly higher than that of the GF (0.80) (**Figure S13, Supporting Information**). The main reason is attributed to the presence of polar -COO^- groups, which can inhibit the transport of ClO_4^- in the electrolyte but favor for the passage of Na^+ [33-34]. Simultaneously, the repulsive force among amyloid fibrils makes it easy to form uniform and stable channels during the film formation process.[35]

2.3. Sodiophilic Mechanism of Amyloid Fibril Components

To understand the outstanding electrochemical behavior of AF-modified separator, we appraised the roles of different groups (leucine: $C_6H_{13}NO_2$, alanine: $C_3H_7NO_2$, and glutamine: $C_5H_{10}N_2O_3$) on AF surface.[36] Density functional theory (DFT) calculations are employed to investigate the Na binding energy of various amino acids in amyloid fibrils, with the aim of elucidating their sodiophilic properties. Detailed insight into the initial and stable adsorption configurations of six different Na adsorption sites is performed for each amino acid, as shown in **Figure 3a-c, Figure S14-16**. It is worth noting that the positions with higher electronegativity have a greater propensity for Na atom adsorption, as shown by the configuration changes during our analyses. Additionally, the interaction of Na atom with the surfaces of leucine or alanine is looser than the interaction of Na atom with the surface of glutamine. The possible reason is related to the small binding energies

between the two amino acids and Na atoms. In contrast, the latter has a large negative binding energy. Evidently, glutamine site 1 has the highest binding energy of -0.449 V for Na atom, indicating that glutamine is the most sodiophilic reason in the amyloid fibril.[13]

To further understand the interaction between amino acids and Na atoms, the charge density difference has been calculated to compare adsorption sites of different amino acids on Na atoms (Site 1). Specifically, the electrons are restricted within the adsorption sites on the leucine and alanine surfaces, weakening the coupling interactions (**Figure 3d-e**). However, the charge transfer from Na to the glutamine site1 is more pronounced, demonstrating the delocalized electron in-between the conjugation structure (**Figure 3f**). In addition, the strong adsorption strength of site 1 can also be elucidated in terms of the two-dimensional electronic structure. According to the (100) crystal plane projection, the glutamine exhibits the highest charge density difference around Na in contrast to leucine and alanine. Correspondingly, the projection on the (010) and (001) planes exhibits a similar situation (**Figure 3g-i, Figure S17, Supporting Information**), indicating that the glutamine in the amyloid fibril has strongest affinity with Na atom.[37]

2.4. Battery Performance

To evaluate the cycling stability of the AF5@GF separator, the symmetric Na||Na batteries were fabricated. **Figure 4a and Figure S18a-b** exhibit the voltage-time curves of Na||Na batteries with different separators at 0.5 mA cm^{-2}. Notably, the batteries with the AF5@GF separator deliver virtually flat voltage plateaus over 1800 h with small overpotential (120 mV), illustrating their good interfacial stability and cyclability. However, for the batteries with the GF separators, the voltage hysteresis seriously plummets after 310 h, indicating that the battery has appeared short circuit. In

addition, the AF has a marginal effect on the overpotential, probably due to the nature of the biomolecule itself, which is common in protein-modified metal cells. [38-41] Inspiringly, we have achieved significant improvements in stabilizing cycle life of Na metal batteries by means of amyloid fibril modified separators in ester-based electrolytes, compared to sodiophilic coating techniques (Al_2O_3, Mg-MOF-74, graphene derivatives, NaBr/Na_3P nanocrystallines) [42-48], three-dimensional Na anode designs (carbonized wood composite) [49], electrolyte modification methods ($C_{60}(NO_2)_6$ additive) [50], and Na alloy modification strategies (Na-Sn alloy) [51], as summarized in **Figure 4b, Figure S18c-h, Figure S19 and Table S1**. Additionally, the batteries with the GF, AF1@GF, AF10@GF separators hardly sustain a current density at 5 mA cm^{-2}, whereas the batteries with the AF5@GF separator survives in the current density ranging from 0.5 to 5 mA cm^{-2}, which can recover to the initial state once the current density returns (**Figure 4c**). Electrochemical impedance spectroscopy (EIS) was also tested after cycling of symmetric cells with the bare GF and the AF5@GF separators at a current density of 0.5 mA cm^{-2} and a capacity of 1 mAh cm^{-2} (**Figure 4d-e, Table S2, Supporting Information**). For symmetric batteries with the GF separator, continuous dendrite growth is detected because of the uneven distribution of Na ions in the battery system, and the accumulated SEI layer with poor Na-ion conductivity leads to high resistance. By comparison, the symmetric batteries with the AF5@GF separator shows a rather stable and consistently low resistance even after 50 cycles, with only one tenth of the resistance of batteries equipped with the GF separator. It indicates the stable interface properties of the AF5@GF during cycling due to its interconnected matrix.

The morphology and composition of the Na surface were investigated using SEM images and XPS tests after disassembling symmetric batteries cycled at a current density of 0.5 mA cm^{-2} and a

capacity of 1 mAh cm^{-2}. As cycled number increased, the anode surface in batteries with the AF1@GF and AF10@GF separators exhibits increasingly inhomogeneous, and dendrites are even observed after 125 and 175 cycles, respectively. Even worse, the dendrites present on the anode with the GF separators after only 10 cycles, and the dendrites growth becomes more severe in the following cycles. (**Figure 4f, Figure S20a-i, Supporting Information**). Attractively, a smooth and dense surface can be still observed on the Na anode of the Na metal battery using the AF5@GF separator, even after 375 cycles (**Figure 4g, Figure S20j-l, Supporting Information**). This further proves that the AF5 can suppress dendrite growth by homogenizing the Na ion concentration, thereby improving the battery cycle stability. Additionally, XPS results suggest that N element in the AF5 is reduced by Na, relative to the formation of Na_3N and NaN_xO_y compounds (**Figure 4h**). The mixed ion-electron mixed conductivity of the reduced products facilitates ion transport, resulting in a uniform ion concentration at the anode-electrolyte interface, which ultimately improves plating/stripping stability of symmetric batteries.[52] It is thought that Na_3N and NaN_xO_y are presented during the cycling process because both of them are hardly detected by XPS before the battery is cycled (**Figure 4h**), consistent with the results obtained from FTIR spectroscopy. This also proves that the AF5 remains stable in the electrolyte prior to cycling and the intensity of the N-containing group peaks of the AF5 decreases relatively after cycling (**Figure S21, Supporting Information**). Conversely, the SEI film constituents, including Na_2CO_3, Na_2O, and NaF, are present on the Na surface even before the battery is cycled, suggesting that these constituents are spontaneously formed *via* the reaction between Na and the electrolyte (**Schematic 1 and Figure S22, Supporting Information**).

To highlight the potential applicability of the modified separator, full cells consisting of 100 μm Na metal anode, a $Na_3V_2(PO_4)_3$ (NVP)@C cathode active materials (mass loading: 5 mg cm^{-2}) and the AF5-coated separator were tested (**Figure 5a, Figure S23a-f, Supporting Information**). Specifically, the long-term durability of Na metal cells with the AF5@GF separator under 1 C has been measured. Evidently, an outstanding cycling stability and discharge capacity retention rate of 87.13% for 1000 cycles is achieved. This performance is far better than that of Na metal full cells assembled with the GF, AF1@GF, and AF10@GF separators, respectively (**Figure 5b**). Moreover, the voltage profiles obtained from cycling the different cells illustrate a single flat charge voltage plateau and two distinct discharge voltage plateaus during the initial cycles (**Figure 5c-d, Figure S23g-h, Supporting Information**). [53-54] The charge voltage plateau is attributed to the extraction of Na ions from the NVP cathode, while the two discharge voltage plateaus are attributed to a two-step Na ion diffusion process resulting from slow Na^+ intercalation kinetics. [53-55] After that, the voltage hysteresis between these two discharge plateaus gradually decreases and these two platforms correspondingly become one upon subsequent cycling. In addition, the voltage hysteresis of the cell assembled with the AF5@GF separator slightly increases to 0.588 V (1000 cycles), while the voltage hysteresis of the cell assembled with the bare GF separator enhances sharply to 0.846 V after just 200 cycles.

Furthermore, the interface evolution of different full cells was investigated by *in-situ* EIS under galvanostatic charge-discharge mode **(Figure 5e, Figure S24, and Table S3, Supporting Information)**. The Na|AF5@GF|NVP full cell shows a notable reduction in the SEI impedance (R_f) from the initial state to the beginning of discharge. Meanwhile, the final R_f is very close to the initial state R_f after discharge, implying good reversibility of the Na|AF5@GF|NVP full cell. Conversely, the Na|GF|NVP full cell exhibits a significant increment in R_f values within a single cycle. Differing from that of the

Na|AF5@GF|NVP full cell, the value of R_f of the Na|GF|NVP full cell at the initially discharged state shows typical irreversible dendrite growth and SEI deterioration. A similar trend has been established in the evolution of the charge transfer impedance (R_{ct}) during the whole cycle. Additionally, the full cell incorporating the AF5@GF separator exhibits superior rate capability compared to those other separators **(Figure 5f)**. The full cell utilizing the AF5@GF separator achieves a discharge capacity of 96.15 mAh g^{-1} at 5C, which is higher than that achieved by cells incorporating the GF, AF1@GF, and AF10@GF separators.

3. Conclusion

In summary, we propose a simple strategy of the separator modified by amyloid fibril biomolecules to achieve homogeneous, compact and reversible sodium metal deposition. It is confirmed that the amyloid fibril can homogenize electric field distribution and ion concentration, reducing the growth of non-densely packed surface crystals. Both experimental and theoretical results indicate that amino acids in the amyloid fibril are strongly sodiophilic, and form stable SEI films during cycling, providing uniform Na ion transport and dendrite-free Na deposition. As a consequence, the modified symmetric cells can be cycled stably for 1800 h at 0.5 mA cm^{-2} under an ester-based electrolyte, overwhelming the majority of similar systems reported so far. Moreover, the Na/$Na_3V_2(PO_4)_3$ full cell containing amyloid fibril can operate for 1000 cycles and maintain a capacity retention of 87.13%. The successful exploration to overcome dendrite-growth in sodium metal batteries demonstrates that the biomolecular-modified separator conception can be promisingly extended to other metal batteries with high reversibility.

Supporting Information

Supporting Information is available from the Wiley Online Library or from the author.

Acknowledgments

We greatly acknowledge the financial support from National Natural Science Foundation of China (52171126, 51971194, and 52202374) and the Natural Science Foundation of Hebei Province for Outstanding Youth Program (E2022203167) and Innovation Groups Program (No. 2022203003). We would like to express our gratitude to Ministry of Education Yangtze River Scholar Professor Program (T2020124) and the Foreign Intelligence Introduction Program of Hebei Province (213000302). In addition, J. M. Wang acknowledge the Hebei Postgraduate Innovation Grant Project (CXZZBS2023048).

References

[1] H. Dai, B. Jiang, X. Hu, X. Lin, X. Wei, M. Pecht, *Renew. Sust. Energ. Rev.* **2021**, *138*, 110480.

[2] M. S. Houache, C.-H. Yim, Z. Karkar, Y. Abu-Lebdeh, *Batteries* **2022**, *8*, 70.

[3] W. Bao, R. Wang, B. Li, C. Qian, Z. Zhang, J. Li, F. Liu, *J. Mater. Chem. A* **2021**, *9*, 20957.

[4] H. Kang, Y. Liu, K. Cao, Y. Zhao, L. Jiao, Y. Wang, H. Yuan, *J. Mater. Chem. A* **2015**, *3*, 17899.

[5] S. Vineeth, C. B. Soni, Y. Sun, V. Kumar, Z. W. Seh, *Trends Chem.* **2022**, *4*, 48.

[6] Z. Li, K. Zhu, P. Liu, L. Jiao, *Adv. Energy Mater.* **2022**, *12*, 2100359.

[7] T. Wang, Y. Hua, Z. Xu, J. S. Yu, *Small* **2022**, *18*, 2102250.

[8] C. Chu, R. Li, F. Cai, Z. Bai, Y. Wang, X. Xu, N. Wang, J. Yang, S. Dou, *Energy Environ. Sci.* **2021**, *14*, 4318.

[9] G. G. Eshetu, M. Martinez-Ibañez, E. Sánchez-Diez, I. Gracia, C. Li, L. M. Rodriguez-Martinez,

T. Rojo, H. Zhang, M. Armand, *Chem. Asian J.* **2018**, *13*, 2770.

[10] Z. Lin, Q. Xia, W. Wang, W. Li, S. Chou, *InfoMat* **2019**, *1*, 376.

[11] J. Liang, Q. Chen, X. Liao, P. Yao, B. Zhu, G. Lv, X. Wang, X. Chen, J. Zhu, *Angew. Chem. Int. Ed.* **2020**, *59*, 6561.

[12] Z. Hou, Y. Gao, H. Tan, B. Zhang, *Nat. Commun.* **2021**, *12*, 1.

[13] Q. Jin, H. Lu, Z. Zhang, J. Xu, B. Sun, Y. Jin, K. Jiang, *Adv. Sci.* **2022**, *9*, 2103845.

[14] J. Wang, Q. Kang, J. Yuan, Q. Fu, C. Chen, Z. Zhai, Y. Liu, W. Yan, A. Li, J. Zhang, *Carbon Energy* **2021**, *3*, 153.

[15] M. Han, C. Zhu, T. Ma, Z. Pan, Z. Tao, J. Chen, *Chem. Commun.* **2018**, *54*, 2381.

[16] Z. Ju, J. Nai, Y. Wang, T. Liu, J. Zheng, H. Yuan, O. Sheng, C. Jin, W. Zhang, Z. Jin, *Nat. Commun.* **2020**, *11*, 1.

[17] Z. Ju, G. Lu, O. Sheng, H. Yuan, S. Zhou, T. Liu, Y. Liu, Y. Wang, J. Nai, W. Zhang, *Nano Lett.* **2022**, *22*, 1374.

[18] J. Zhi, S. Li, M. Han, P. Chen, *Sci. Adv.* **2020**, *6*, eabb1342.

[19] M. Liu, L. Jia, Z. Zhao, Y. Han, Y. Li, Q. Peng, Q. Zhang, *Chem. Eng. J.* **2020**, *390*, 124667.

[20] A. Barth, *Biochim. Biophys. Acta Gen. Subj.* **2007**, *1767*, 1073.

[21] Q. Zhang, Q. Yang, P. Phanlavong, Y. Li, Z. Wang, T. Jiao, Q. Peng, *ACS Sustain. Chem. Eng.* **2017**, *5*, 4161.

[22] B. Wang, J. Xia, L. Mei, L. Wang, Q. Zhang, *ACS Sustain. Chem. Eng.* **2018**, *6*, 1343.

[23] G. Li, Z. Liu, Q. Huang, Y. Gao, M. Regula, D. Wang, L.-Q. Chen, D. Wang, *Nat. Energy* **2018**, *3*, 1076.

[24] Q. Zhang, S. Zhang, Z. Zhao, M. Liu, X. Yin, Y. Zhou, Y. Wu, Q. Peng, *J. Clean. Prod.* **2020**, *255*,

120297.

[25] X. Liu, N. Zhang, L. Yu, S. Zhou, R. Shanks, J. Zheng, *Food Hydrocoll.* **2016**, *60*, 7.

[26] W. Sun, Q. Zhao, M. Zhao, B. Yang, C. Cui, J. Ren, *J. Agric. Food Chem.* **2011**, *59*, 11070.

[27] C. Lara, J. Adamcik, S. Jordens, R. Mezzenga, *Biomacromolecules* **2011**, *12*, 1868.

[28] J. Wang, Z. Xu, Q. Zhang, X. Song, X. Lu, Z. Zhang, A. J. Onyianta, M. Wang, M. M. Titirici, S. J. Eichhorn, *Adv. Mater.* **2022**, *34*, 2206367.

[29] Q. Zhao, Y. Deng, N. W. Utomo, J. Zheng, P. Biswal, J. Yin, L. A. Archer, *Nat. Commun.* **2021**, *12*, 1.

[30] L. Geng, Q. Liu, J. Chen, P. Jia, H. Ye, J. Yan, L. Zhang, Y. Tang, J. Huang, *Nano Res.* **2022**, *15*, 2650.

[31] J. Newman, K. E. Thomas, H. Hafezi, D. R. Wheeler, *J. Power Sources* **2003**, *119*, 838.

[32] K. E. Thomas-Alyea, J. Newman, G. Chen, T. J. Richardson, *J. Electrochem. Soc.* **2004**, *151*, A509.

[33] Y. Yang, Z. Chang, M. Li, X. Wang, Y. Wu, *Solid State Ion.* **2015**, *269*, 1.

[34] H. Zhou, J. Gu, W. Zhang, C. Hu, X. Lin, *Molecules* **2021**, *26*, 5539.

[35] D. Lv, J. Chai, P. Wang, L. Zhu, C. Liu, S. Nie, B. Li, G. Cui, *Carbohydr. Polym.* **2021**, *251*, 116975.

[36] S. Bolisetty, R. Mezzenga, *Nat. Nanotechnol.* **2016**, *11*, 365.

[37] Z. Li, K. Zhu, P. Liu, L. Jiao, *Adv. Energy Mater.* **2022**, *12*, 2100359.

[38] L. Nie, Y. Li, S. Chen, K. Li, Y. Huang, Y. Zhu, Z. Sun, J. Zhang, Y. He, M. Cui, *ACS Appl. Mater. Interfaces* **2019**, *11*, 32373.

[39] X. Fu, R. Odstrcil, M. Qiu, J. Liu, W.-H. Zhong, *Energy Storage Mater.* **2021**, *42*, 22.

[40] B. Zhang, H. Shi, Z. Ju, K. Huang, C. Lian, Y. Wang, O. Sheng, J. Zheng, J. Nai, T. Liu, *J. Mater.*

Chem. A **2020**, *8*, 26045.

[41] T. Wang, Y. Li, J. Zhang, K. Yan, P. Jaumaux, J. Yang, C. Wang, D. Shanmukaraj, B. Sun, M. Armand, *Nat. Commun.* **2020**, *11*, 5429.

[42] W. Luo, C. F. Lin, O. Zhao, M. Noked, Y. Zhang, G. W. Rubloff, L. Hu, *Adv. Energy Mater.* **2017**, *7*, 1601526.

[43] Y.-J. Kim, H. Lee, H. Noh, J. Lee, S. Kim, M.-H. Ryou, Y. M. Lee, H.-T. Kim, *ACS Appl. Mater. Interfaces* **2017**, *9*, 6000.

[44] M. Zhu, S. Li, B. Li, Y. Gong, Z. Du, S. Yang, *Sci. Adv.* **2019**, *5*, eaau6264.

[45] H. Wang, C. Wang, E. Matios, W. Li, *Nano Lett.* **2017**, *17*, 6808.

[46] T. Yang, T. Qian, Y. Sun, J. Zhong, F. Rosei, C. Yan, *Nano Lett.* **2019**, *19*, 7827.

[47] Z. Luo, S. Tao, Y. Tian, L. Xu, Y. Wang, X. Cao, Y. Wang, W. Deng, G. Zou, H. Liu, *Nano Energy* **2022**, *97*, 107203.

[48] Y. Zhao, L. V. Goncharova, Q. Zhang, P. Kaghazchi, Q. Sun, A. Lushington, B. Wang, R. Li, X. Sun, *Nano Lett.* **2017**, *17*, 5653.

[49] W. Luo, Y. Zhang, S. Xu, J. Dai, E. Hitz, Y. Li, C. Yang, C. Chen, B. Liu, L. Hu, *Nano Lett.* **2017**, *17*, 3792.

[50] P. Li, Z. Jiang, X. Huang, X. Lu, J. Xie, S. Cheng, *Nano Energy* **2021**, *89*, 106396.

[51] X. Zheng, W. Yang, Z. Wang, L. Huang, S. Geng, J. Wen, W. Luo, Y. Huang, *Nano Energy* **2020**, *69*, 104387.

[52] Q. Shi, Y. Zhong, M. Wu, H. Wang, H. Wang, *Angew. Chem. Int. Ed.* **2018**, *57*, 9069.

[53] L. Chen, Y. Zhao, S. Liu, L. Zhao, *ACS Appl. Mater. Interfaces* **2017**, *9*, 44485.

[54] C. Wei, F. Luo, C. Zhang, H. Gao, J. Niu, W. Ma, Y. Bai, Z. Zhang, *Ionics* **2020**, *26*, 2343.

[55] X. Li, Y. Huang, J. Wang, L. Miao, Y. Li, Y. Liu, Y. Qiu, C. Fang, J. Han, Y. Huang, *J. Mater. Chem. A* **2018**, *6*, 1390.

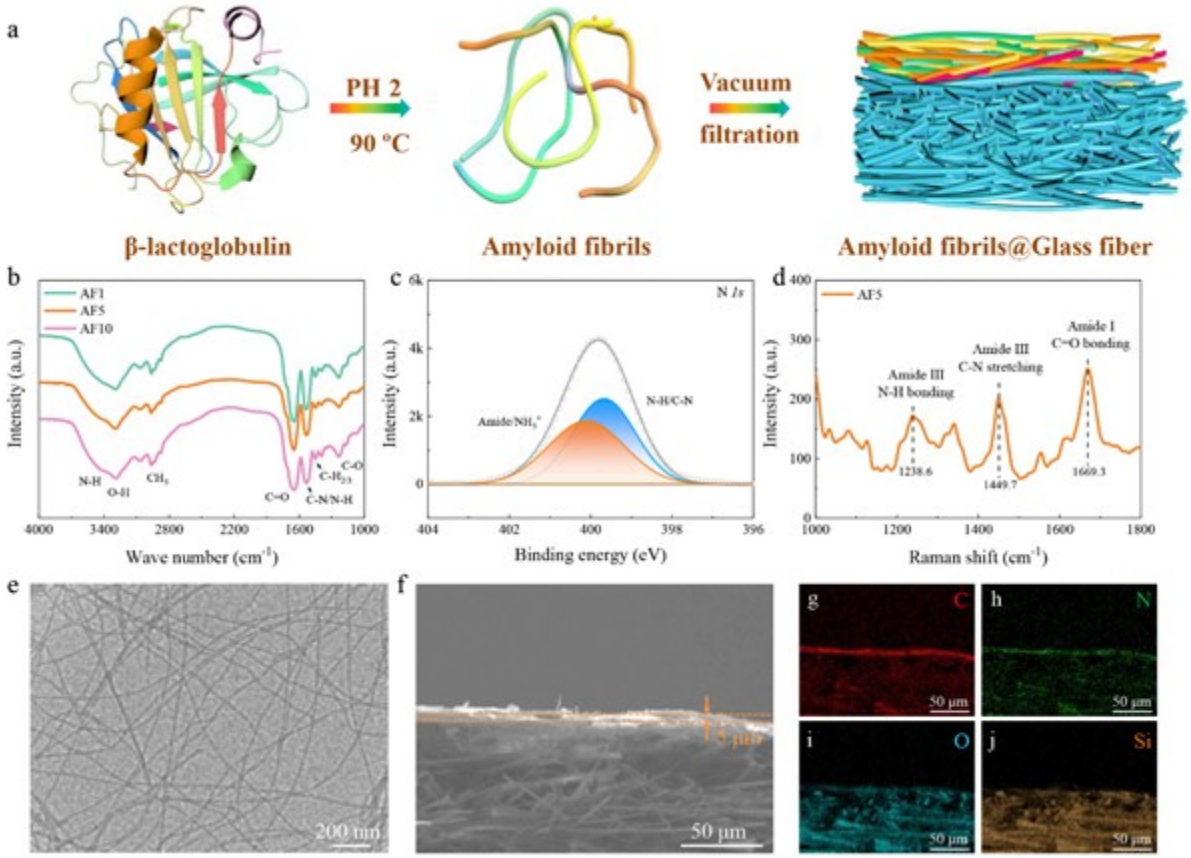

Figure 1. (a) Schematic illustration of the synthetic process of the AF5@GF separator. (b) FT-IR patterns of AF1, AF5, and AF10. (c) XPS profiles of the AF5 in N *1s* spectrum. (d) Raman spectrum of the AF5. (e) TEM image of the AF5. (f-j) Longitudinal-section SEM image and corresponding mapping of the AF5@GF separator.

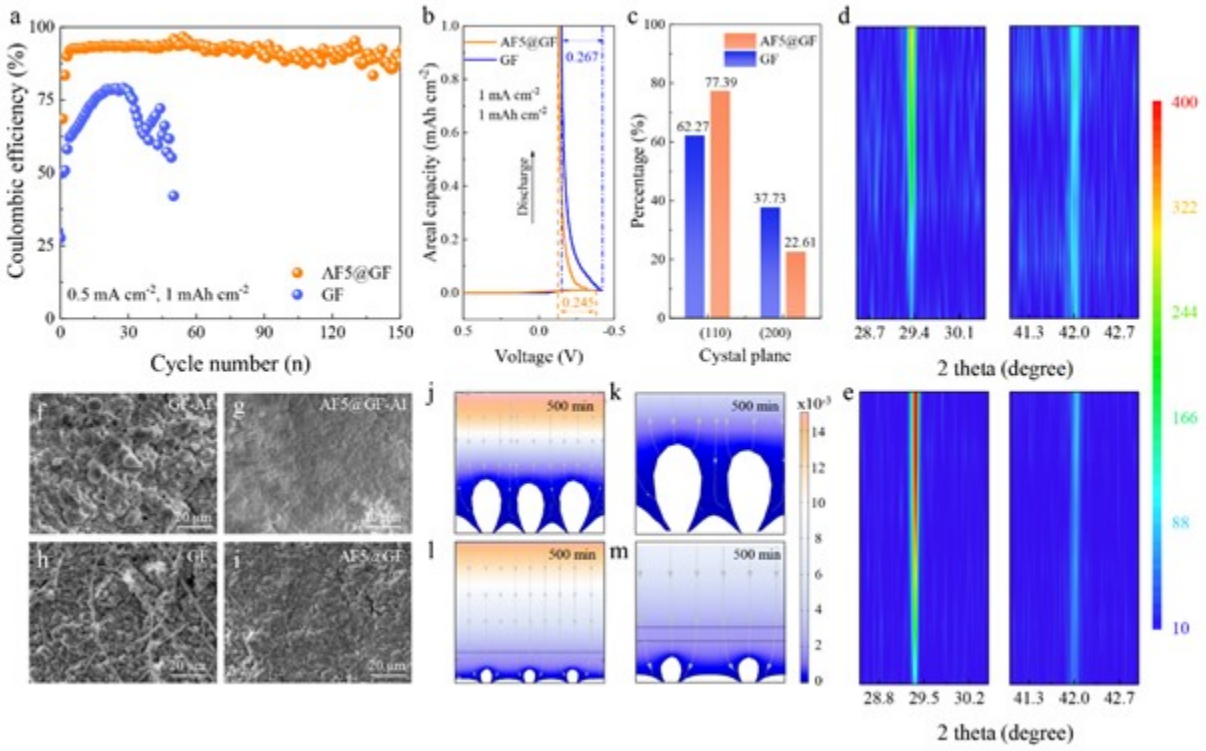

Figure 2. (a) Coulombic efficiency of different separator at 0.5 mA cm^{-2} and 1 mAh cm^{-2}. (b) Voltage profiles of Na nucleation under different separator at 1 mA cm^{-2}. (c) Percentage of (110) and (200) crystalline surfaces of Na deposited under different separator. (d-e) *In-situ* XRD patterns of Na deposition processes in Na|Al half-cells with GF separator (d) or AF5@GF separator (e). (f-g) Na deposition on Al current collector using GF separator (f) or AF5@GF separator (g). (h-i) Na deposition on the GF separator (h) or the AF5@GF separator (i). (j-m) Simulate the electric field distribution on Na anode without AF5 (j-k) and with AF5 (l-m) after 500 min.

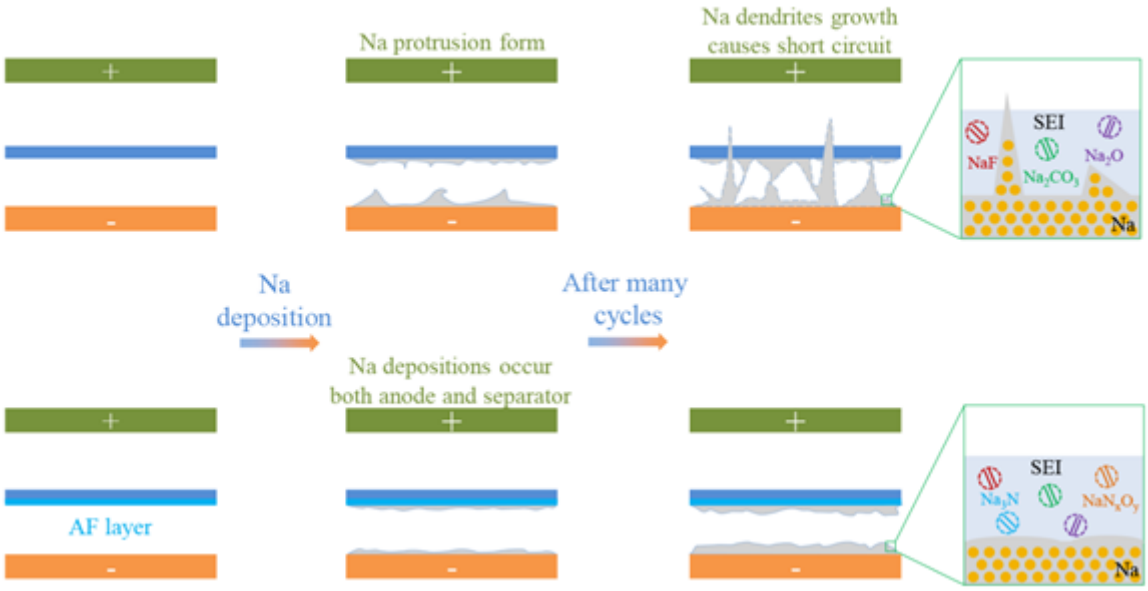

Scheme 1. Schematic representation of Na growth in Na cells before and after amyloid fibrils modification.

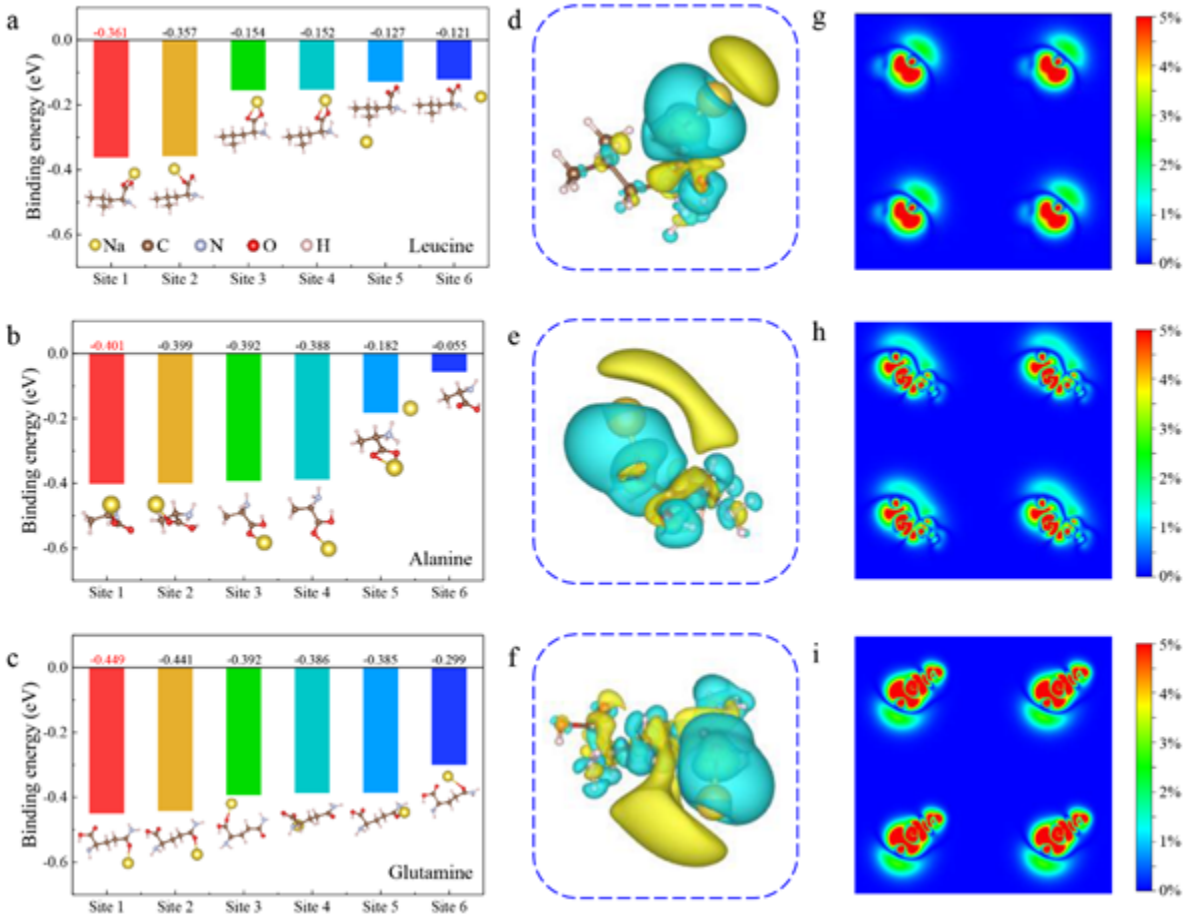

Figure 3. (a-c)Summary of calculated binding energies of Na with leucine, alanine, and glutamine in amyloid fibril. (Inset: Stable structure model after Na adsorption at different sites) The Na, C, N, O, and H atoms are marked as yellow, brown, blue, red, and pink, respectively. (d-f)The (100)plane of the three-dimensional charge density differences with isosurface value of 0.01 e/Bohr^3 of (d)leucine, (e)alanine, and (f)glutamine with one Na atom adsorbed. Blue and yellow colors represent losing and gaining electrons, respectively. (g-i)The electronic charge density differences contour plots on (100)plane of (g) leucine, h) alanine, and (i) glutamine with one Na atom adsorbed.

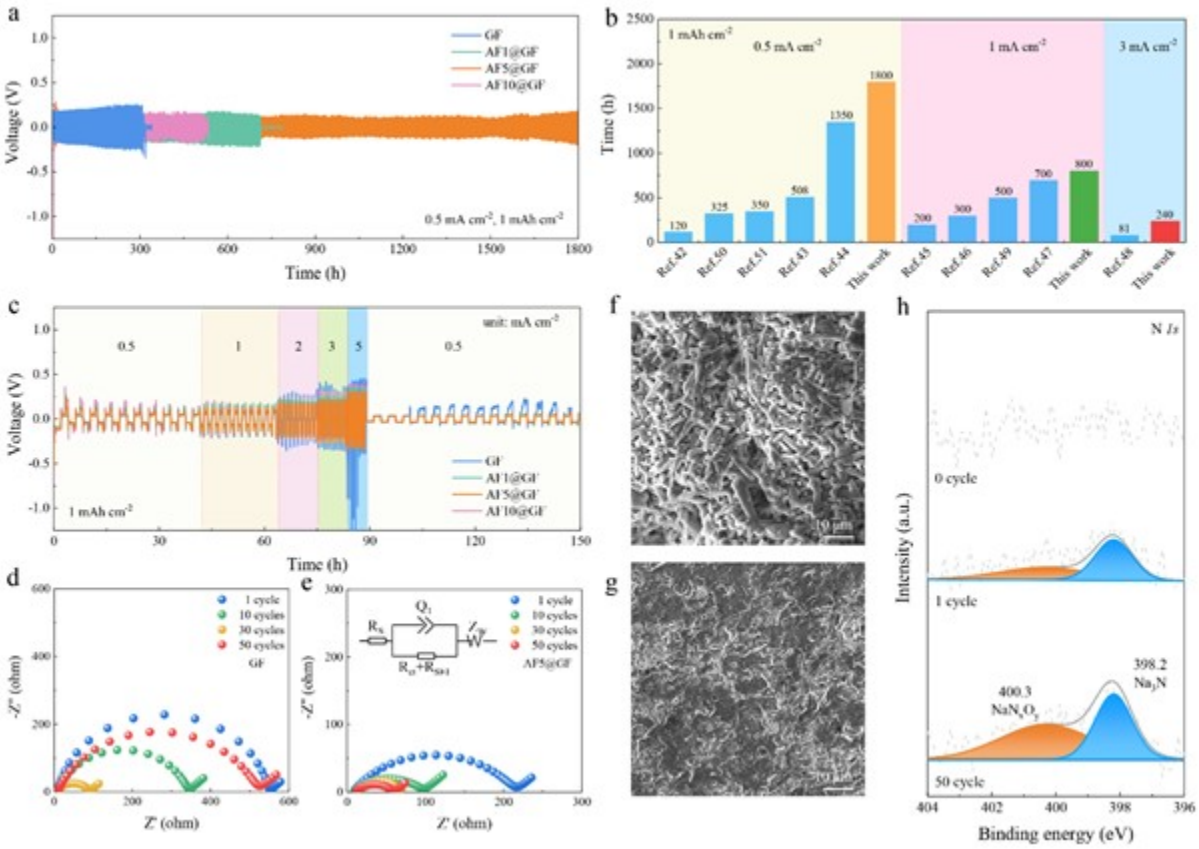

Figure 4. (a) Voltage time profiles of Na plating/stripping process at 0.5 mA cm^{-2} with 1.0 mAh cm^{-2}. (b) Comparison of cycle times of sodium batteries equipped with AF5@GF separator with other reported sodium batteries at different current densities in ester-based electrolyte. (c) Rate performances of symmetric batteries using different separators at various current density from 0.5 to 5 mA cm^{-2} with a stripping/plating capacity of 1 mAh cm^{-2}. (d-e) EIS values of Na symmetric batteries with GF separators (d) or AF5@GF separators (e) after different cycles. The inset is the EIS fitting circuit diagram. (f-g) Na surface SEM morphology of Na symmetric battery after 50 cycles with GF separator (f) and 375 cycles with AF5@GF separator (g). (h) The N*1s* spectrum of the Na surface after 0, 1, and 50 cycles of batteries equipped with AF5@GF separators.

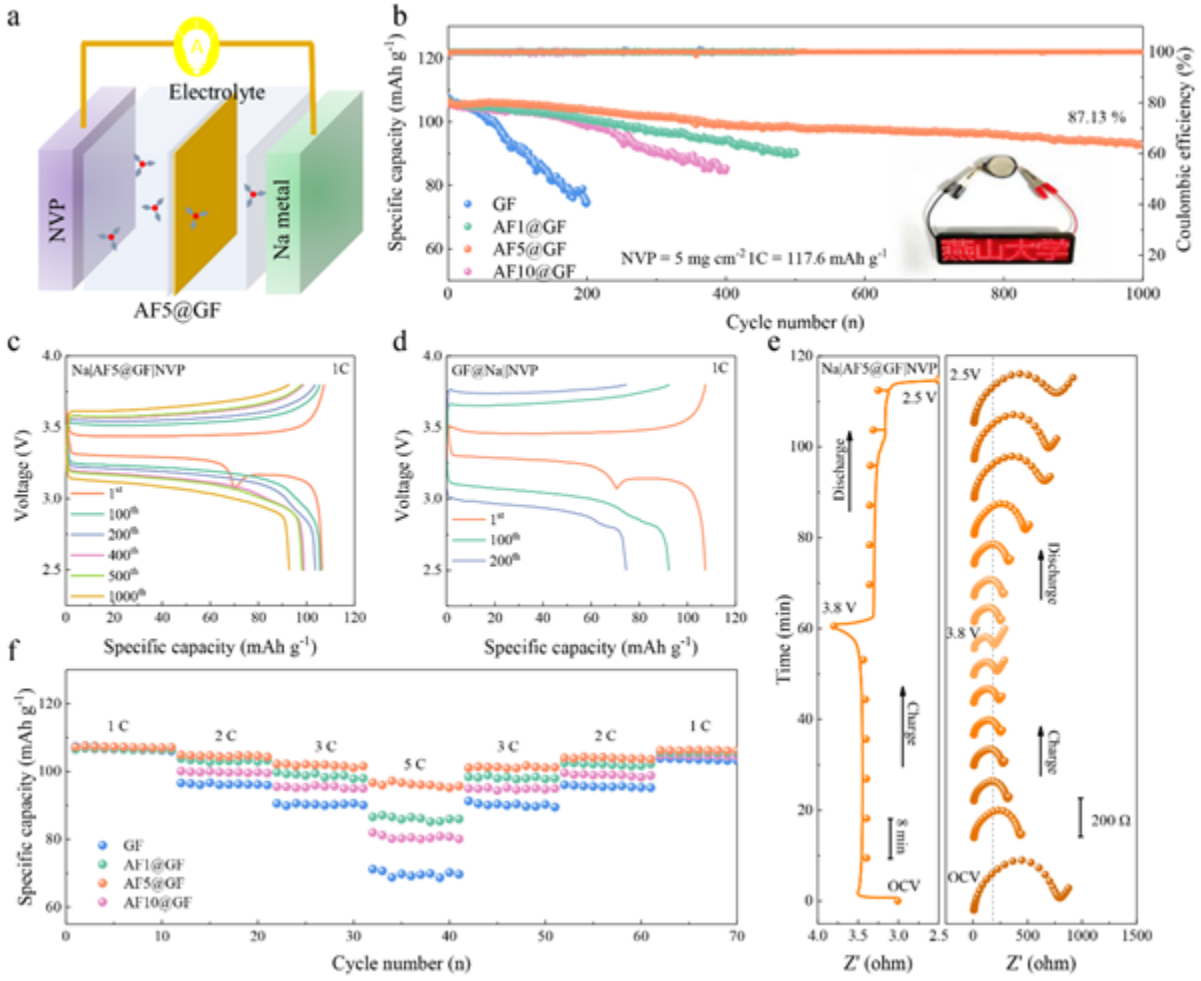

Figure 5. (a) Schematic diagram of a Na metal full cell. (b) Long-term cycling performance at a specific current of 1C. (c-d) A discharge/charge voltage profiles of the full cells of the Na|AF5@GF|NVP (c) and Na|GF|NVP (d). (e) *In-situ* EIS results of the Na|AF5@GF|NVP. (f) Rate capability of the various full cells.

Table of Contents

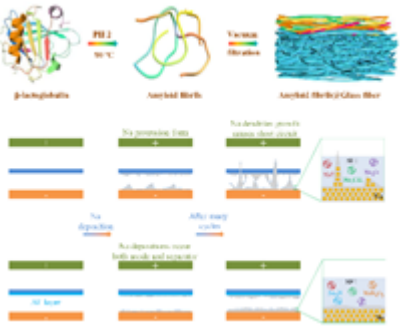

50 × 55 mm

A novel composite separator is fabricated through the vacuum filtration technique, incorporating a unique amyloid fibril onto a glass fiber separator. The composite separator demonstrates remarkable efficacy in suppressing the growth of sodium dendrites due to the formation of a stable solid-electrolyte-interphase film enriched with nitride, which showcasing its potential as a promising solution in sodium battery technology.